Peng Han[1], Jiandong Liu[1*,2,3], Yawen Li[1],Haibing Ruan[1], and Wentao Duan[1]

[1] School of Remote Sensing and Geomatics Engineering, Nanjing University of Information Science and Technology, Nanjing 210044, China.

[2] Laboratoire de Météorologie Dynamique, IPSL Sorbonne Université, Paris 75252, France.

[3] Key Laboratory of Planetary Science, Shanghai Astronomical Observatory, Chinese Academy of Sciences, Shanghai 200030, China.

Corresponding author: J.Liu (jd_liu@nuist.edu.cn)

Key Points:

- Both nightside and dayside density have strong responses to the solar flares
- The density increases 2 to 5 times (150-250 K in temperature) than background values at altitudes above 170 km
- The Mars crustal magnetic field can influence the background thermospheric thermal structure.

Abstract

Mars thermosphere is responsive to solar activities. Previous studies have not examined the neutral density responses to the solar flares thoroughly due to lack of observations. In this paper, Martian thermospheric mass density responses to the February and March 2017 C4.1 and B3.3 solar flare-induced Extreme Ultraviolet (EUV)-enhancement are studied using *Mars Atmosphere and Volatile EvolutioN* (MAVEN) accelerometer (ACC)-derived observations. We focus on analyzing the relationship between the reactions of density and the solar flare indexes. Firstly, the density experiences 2 to 5 times increases during the event, which is equivalent to a temperature increment of 150 to 250 K. Secondly, both nightside and dayside density rise with the EUV-enhancement, which is coupled with the solar flares at all the observed latitudes. Thirdly, the Martian Crustal Magnetic Field (CMF) could alter the thermospheric background thermal structure, which might also have influence on the heating-process caused by the EUV-enhancement. The nightside density inflation during the February event is due to day-night atmospheric transport, while the dayside density expansion is heated by EUV (17-22 nm)-enhancement during the March event directly. The region with an intensive CMF magnitude could restrain the precipitating ions,resulting in cooling of the atmosphere in that area. The thermal structure perturbations caused by these flares-induced EUV-enhancement might trigger considerable augmentation of the Jeans Escape rates of some light volatiles, such as atomic Hydrogen (H) or even short-term hydrodynamic escape in some extreme cases.

Plain Language Summary

Solar flares are sudden increased flash on the Sun surface (accurately, from the region called solar corona). The process is always coupled with massive energy release that can impacts the electromagnetic circumstances of the upper atmosphere in a planet such as Earth and Mars. In this paper, we study two moderate solar flare cases' impacts on the Mars thermospheric density using the observations from the MAVEN spacecraft. The density increases 2-5 times than the average values during the cases, which is caused by the enhancements of X-ray and EUV irradiations induced by the flares. We find that the irradiations can heat the dayside atmosphere, and the heating can be transmitted to the nightside thus causes a sudden increase of density nearby the day-night terminator. Another interesting thing is that the Mars Crustal Magnetic Field (CMF, Mars lacks magnetic dipole field) could alter the global density distributions by restrain the ions precipitating (also can heat the atmosphere then results in density increases) in the upper atmospheric system. Therefore, the CMF might also have influence on the flare-induced heating process.

1 Introduction

Solar events, which are mostly driven by active solar flares, can affect the upper structure of the solar-system terrestrial planets such as Mars (Cravens et al., 2017). The solar flare activities have a huge impact on the Martian upper layers, which leads to massive atmospheric loss (e.g., Jakosky et al., 2015; Thiemann et al., 2015; Elrod et al., 2018; Jain et al., 2018). Both long-term (e.g., 11-yr solar cycles) and temporary solar Extreme Ultraviolet (EUV) radiation variations could drive significant atmospheric responses in the Mars upper layers by ionizing, disassociating, and heating the volatiles through various photochemical processes (Cravens et al., 2017; Jakosky et al., 2018; Martinez et al., 2019).

However, the Martian thermospheric density responses to the solar flare event are not well understood in term of in-situ observations. The mass spectrometer such as *Neutral Gas and Ion Mass Spectrometer* (*NGIMS*) on *Mars Atmosphere and Volatile Evolution Mission* (*MAVEN*) is always turned off to avoid damage caused by the dramatic changes of the electromagnetic circumstance during the event (Stone et al., 2018). Additionally, aerobraking to retrieve mass density from accelerometer does not take place either during those intense solar activities such as M5.8 and X8.2 events (Zurek et al., 2017; Elrod et al., 2018; Fang et al., 2019), which has been well studied by previous work (Jakosky et al., 2015). Moreover, moderate solar flares' (i.e., B and C class) impacts on the Mars upper atmosphere have been not yet fully studied due to lack of observations, especially the density-thermal responses to the coupling EUV enhancement during the event.

Currently, vital progress has been made in studying M and X-class solar flares' effects on the Martian upper atmosphere by both MAVEN observations and MHD simulations (Curry et al., 2015; Fallows, et al., 2015; Ma et al, 2004, 2014). Mars dayside upper atmospheric species abundance increases and vanishes rapidly during the M and X-class flares (Elrod et al., 2018; Thiemann et al., 2015). Thermospheric temperatures increased by ~270-310 K during the

X-class flare on 10^{th} September 2017 and the flare-induced heating is limited to the low and middle latitudes (Jain et al., 2018). The density of CO_2, CO and $O_2{}^+$ inflates at altitudes higher than 100 km during the period of intense solar activities (Lollo et al.,2012; Fallows et al.,2015). The Interplanetary Coronal Mass Ejection (ICME) coupled with the March 2015 M5.8 solar flare causes changes in bow shock and generates widespread diffuse aurora (Jakosky et al., 2015). A Magnetohydrodynamical (MHD) simulation using the September 2019 X8.2 solar flare scenario shows that such X-class event can trigger massive loss of the Martian upper atmosphere (Fang et al., 2019). However, the moderate flares' impacts on the Mars upper atmosphere are rarely considered by current investigations.

In this paper, we investigate two moderate solar flares with EUV enhancements to study their impacts on Martian thermospheric density. The paper is organized as follows: The in-situ observations made by MAVEN and other data used in this article during the two flares' periods are introduced in Section 2 and 3. The density responses to the flares as well as the role of magnetic crustal filed during these interactions are shown in Section 4. A short discussion is listed in Section 5. A detailed summary is made in Section 6.

2 Materials and Methods

2.1 MAVEN instruments to observe solar flares

This study uses comprehensive in-situ MAVEN observations to analyze the accelerometer-derived density's responses to the moderate C4.1 and B3.3 of February and March 2017 solar flares (Figure 1). The coupling enhancements of the solar fluxes in 0.1-7 nm (soft X-rays) and 17-22 nm (EUV) bands are observed (Figure 2). The Martian Crustal Magnetic Field (CMF) effects on such events have also been evaluated. The density data is derived from MAVEN accelerometer (ACC)-measured atmospheric force during the aerobraking phase (Zurek et al.,2015, 2017). The electromagnetic and plasmatic disturbances produced by solar flares are recorded by the Solar Wind Electron Analyzer (SWEA), Solar Energetic Particle (SEP), Extreme Ultraviolet (EUV) monitor and Magnetometer (MAG), respectively (Figure 2).

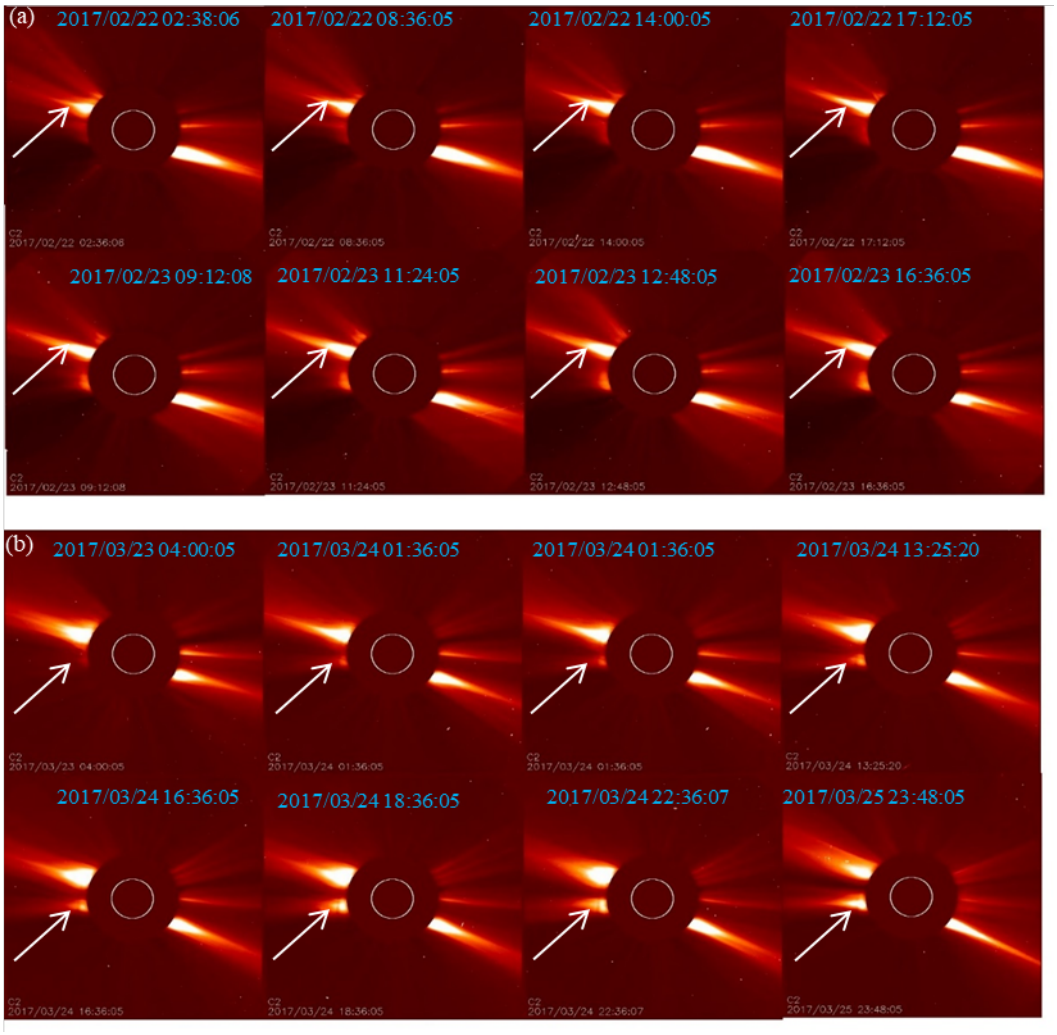

Figure 1. LASCO (the Large Angle and Spectrometric Coronagraph) photos recorded by C2 telescopes on-board the SOHO (Solar and Heliospheric Observatory) satellite are shown during the two events in this paper. The changes of the coronal streamers are shown during the (a) February and (b) March event. The white arrows point to the corona where the solar flares eject out during the periods.The data is available on https://lasco-www.nrl.navy.mil/daily_mpg/.

The instruments have been widely used to evaluate the intensity of the solar activities (e.g., Curry et al., 2015; Fang et al.2019; Martinez et al., 2019; Romanelli et al., 2018, 2019). The SWEA, SEP and MAG monitor are all the parts of the Particles and Fields (PF) Package (Connerney et al., 2015). The SWEA deduces magneto-plasma topology in and above the Martian ionosphere based on electron spectra and pitch angle distributions and measures

atmospheric electron impact ionization effects. SEP instrument determines the impact of SEPs on the upper atmosphere. The MAG measures interplanetary and ionospheric magnetic fields. The EUV monitor is a part of the Langmuir Probe and Waves (LPW) instrument and measures solar EUV input, variability, and wave heating of the Martian upper atmosphere (Andersson et al., 2015). All the data can be downloaded from the MAVEN Science Data Center (https://lasp.colorado.edu/maven/sdc/public/pages/datasets/) and the key parameter data page (https://lasp.colorado.edu/maven/sdc/public/pages/plots/kp/kp.html).

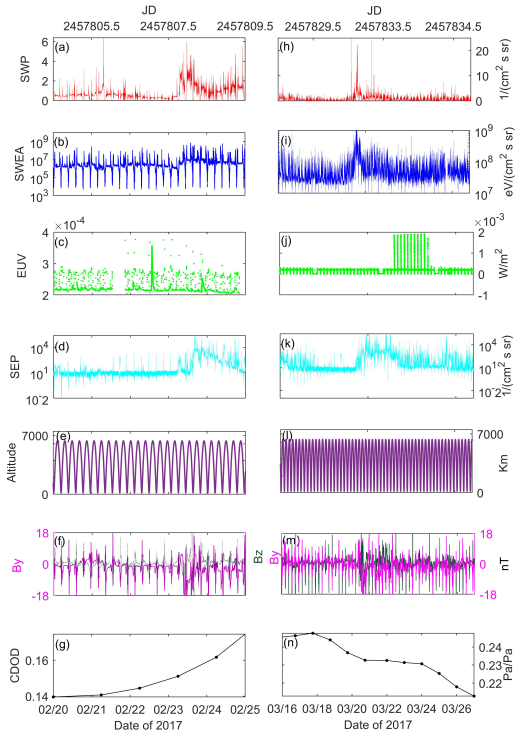

Figure 2. The February (left column) and March (right column) solar flare events are shown as captured by MAVEN observations. We choose the related detectors to represent the intensity of solar event including SWP (a, h), SWEA (b, i), EUV (c, j), SEP (d, k) and MAG (f, m). The orbit data (e, l) illustrate the orbital change effect. The Infrared Column Dust Optical Depth, IR-CDOD (g, n) represents the intensity of surface dust storms (Montabone et al., 2019).

2.2 Observational implementation of the EUV monitor

The LPW instrument onboard the MAVEN integrates the solar EUV monitor, which provides in- situ EUV observations in three bands (Andersson et al., 2015; Jakosky et al., 2015) .The three bands is to characterize EUV resources from

significantly different regions of the solar atmosphere (Thiemann et al., 2017): The 0.1-7 nm band (soft X-rays) represents the irradiance from hot coronal sources and solar flares, while the 17-22 nm band measures from the relatively cooler non-flaring corona. The 121.6 nm measures the bright H I Lyman line, which is originated from the neutral H of solar chromosphere and the interplaneatary transition region (Cravens et al., 2017).

Different bands of EUV radiation behaves in different fashion during various levels of solar events (Figure 2). Current studies on Martian atmospheric responses to solar flares are highly relied on the MHD simulations due to the shutdown of instruments during the events (Ma et al, 2004, 2014; Curry et al., 2015; Fallows, et al., 2015; Jakosky et al., 2015). Therefore, we choose the moderate events, i.e, February and March 2017 solar flares rated for C4.1 and B3.3 with EUV enhancement, to study the interaction between the solar inputs and the Martian upper atmosphere. The class of the solar flares can be obtained from https://www.spaceweatherlive.com/en/archive.html.

3 Accelerometer-derived density and dust storms IR-CDOD index

3.1 Accelerometer-derived density

Thermospheric mass density can be derived from ACC-observed along-track drag forces during aerobraking phase (Zurek et al., 2015), which has been used by early Martian exploration program (Withers and Paul, 2006). Unlike mass spectrometer, the ACC is rarely influenced by the dramatic electromagnetic changes during the moderate solar flare events (Figure 3). Therefore, the ACC-derived density is suitable for investigating the structure responses of the Martian upper layers to the solar flares.

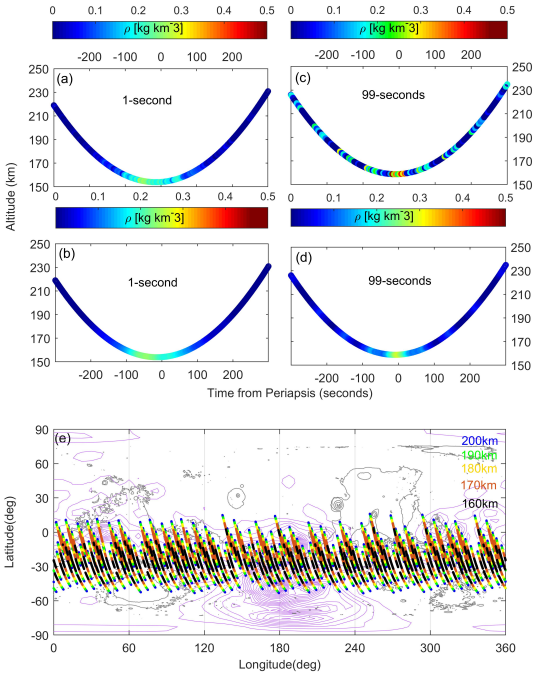

Figure 3. ACC-derived density profiles nearby the MAVEN orbital periapsis. (a) and (b) represent the 1-second samples and 99-seconds average density on February 1st, 2017, respectively. (c) and (d) represent the density during the first day of the February solar flare event (February 22nd, 2017). (e) shows the spatial distribution of the density at different altitudes. The CMF and topographic contour are drawn in the (e) with purple and black line, respectively.

We use MAVEN ACC-derived density to study the responses of the Martian upper atmosphere to the February and March 2017 solar flares (Figure 1 and 2). All the ACC data is available on the NASA Planetary Data System (PDS) (https://atmos.nmsu.edu/PDS/data/PDS4/MAVEN/acc_bundle/l3). The accuracy of the measurement at different altitudes is shown in former research (Zurek et al., 2015, 2017; Liu et al., 2019). The density at altitudes of 160 to 190 km has good global coverage and appropriate accuracy. The ACC-derived density is processed using LMD-MCD (Laboratoire de Météorologie Dynamique Mars Climate Database V5.3) to get the altitude-normalized observations so we can analyze the influence at a specific altitude (Liu et al., 2019; Li et al., 2021).

3.2 Dust storms by IR-CDOD index

As mentioned above, dust storm exists as an important factor affecting the struc-

ture of the atmosphere. To prove that these density changes are not due to dust storms, we also use the Infrared Column Dust Optical Depth (IR-CDOD) to illustrate the corresponding dust storm activities. Figure 2 illustrates the related dust storm activities. The IR-CDOD dataset can be found at http://www-mars.lmd.jussieu.fr/mars/dust_climatology/index.html from MY24 to MY33 (Montabone et al., 2019). The IR-CDOD is below 0.25 Pa/Pa in Figure 2, which implies the activities of the surface dust storm are inactive.

4 Results

4.1 Long-term variations driven by the seasonal variables

The Martian upper atmosphere experiences a strong seasonal cycle due to the relatively larger eccentricity of Mars evolution orbit around the Sun, the obliquity of its rotation axis (similar with Earth), and the close of the apsides with the solstices (Forget et al.,2009; Zurek et al., 2017; Liu et al., 2019). At a given altitude or horizontally, the seasonal upper atmospheric density varies as follows (Liu et al., 2019):

$$\ln \rho = \alpha_0 + \frac{\alpha_1 cosSZA + \alpha_2}{r_{\mathrm{sm}}^2} + \alpha_3 IR\_CDOD_{\mathrm{dust}} \quad (1)$$

Where $\ln \rho$ is the natural logarithm of density ρ. cosSZA, cosine of Solar Zenith Angle. r_{sm}^2, square of the Sun-Mars distance. IR_CDOD_{dust} is the dust storm index (Montabone et al., 2019). α_0 to α_3 are parameters. Fitting has been made to show this long-term trend. The results are illustrated in Figure 4 (gray dots) and the parameters are listed in Table 1.

Table 1. Model Fitting Coefficients of ACC Data at Different Altitudes by Equation (1)

Coefficients Altitude(km)	α_0	α_1	α_2	α_3

The background density of Mars upper layer is governed by equation (1) horizontally and fulfills Hydrostatic Equilibrium (HE) vertically, i.e., density decreases with altitude exponentially (Figure 4). Except these two background drivers cause long-term trends (gray point in Figure 4b and 4c), there are other variations such as gravity waves caused by couple of factors existing during Mars evolution. These variations have complex longitudinal-latitudinal structures as described by former research (Liu et al., 2019; Li et al., 2021). To highlight the density changes during the solar flare events, we use brown color to tag out the observations in that period (Figure 4).

As illustrated in Figure 4a and 4d, the density follows the HE vertically. Horizontally, the mechanism implied by equation (1) dominates the density variations at a given altitude below 170 *km* (Figure 4b and 4c). The density amplitudes approximate the same as in common situations at these lower altitudes. The density increases during the events are not obvious.

However, the density is obviously higher than the average (seasonal trend) when the altitude is greater than 180 *km*. It is shown that the atmosphere is indeed heated during these events. Additionally, the derived errors of the density show sharp increases synchronously as seen in Figure 5. It is well worth noting that the observation made during the first event (Figure 4b) is in the nightside (SZA >90°), while densities during the second event (Figure 4c) lies on the dayside (SZA < 90°).

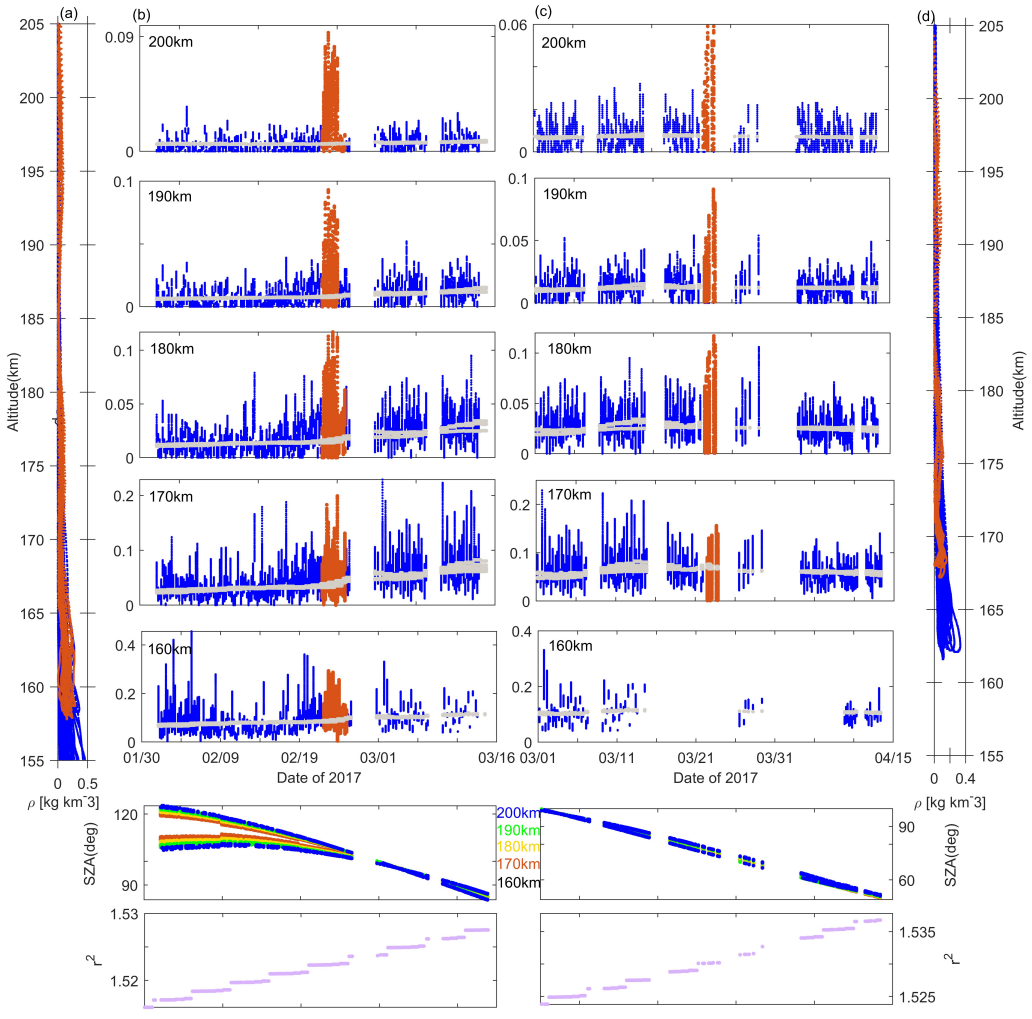

Figure 4. The vertical and horizontal profiles of the density are shown during the two events: (a) vertical and (b) horizontal density profiles during the February event. (c) and (d) is the same as (b) and (a) but for the March. The blue points represent the background densities and the brown dots are the densities when the two events happened. The gray spots show the fitting results based on equation (1). The fitting parameter SZA (inbound and outbound) and $r^2_{\rm sm}$ are also drawn on the bottom panels.

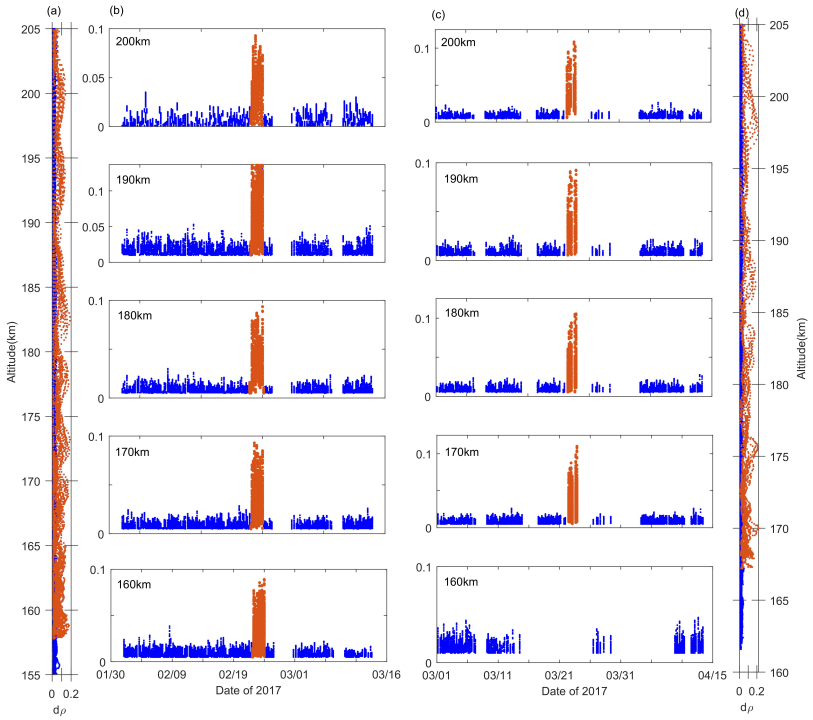

Figure 5. same as Figure 4 but for derived errors.

4.2 Density responses to the 22$^{\rm nd}$ February 2017 C4.1 Solar Flare

The hot solar flare, which starts at ~14:14 20$^{\rm th}$ February 2017 as shown in Table 2, triggers a solar flare series from B3.0 to C4.1 during the next few days (Table 2). The sensors on the MAVEN spacecraft capture the flickering of these flares as shown in Figure 2. The EUV enhancement on 22$^{\rm nd}$ February is triggered by a flaring hot solar corona as shown in Figure 1.

Table 2. The Solar Flare Series during 20$^{\rm th}$ to 24$^{\rm th}$ February 2017

Flare-Class Stage(UTC)	B7.5 2.20	B3.0 2.21	**C4.1 2.22**	**C1.3 2.23**	**C1.1 2.24**	B3.2 2.26
Start	:14	:14	**13:03**	**20:43**	**00:04**	:11
Maximum	:25	:22	**13:27**	**20:53**	**00:12**	:18
End	:32	:26	**13:38**	**21:11**	**00:14**	:25

Figure 6 shows the ACC density (Figure 6a to 6e) and the related indexes (Figure 6f to 6l) during the February 2017 C4.1 Solar Flare event. The Martian thermospheric density increases 2 to 4 times higher than the long-term background trends as driven by the factors in equation (1). The indexes represented by SWP, By, SEP, and SWEA share a similar trend during the period, which implies that the solar winds and the Interplanetary Magnetic Field (IMF) have minor contribution in enhancing the Mars thermospheric density during this event series (Table 2) as expected. The surface dust storms are also relatively calmer at the end of a Mars Year (MY33, Ls 308°-336°)(Montabone et al., 2019). The density is heated by the 0.1-7 nm X-rays enhancement, i.e., EUV (0.1-7 nm) (Figure 6f), increasing from 2.25×10^{-4} to almost 3×10^{-4} W m^{-2} as illustrated in Figure 6f. The event series are caused by the emissions from a hot solar corona within a few days as shown in Figure 1, which are not revealed by 11-17 nm wavelength band that is designed to capture the activities from relatively cooler corona.

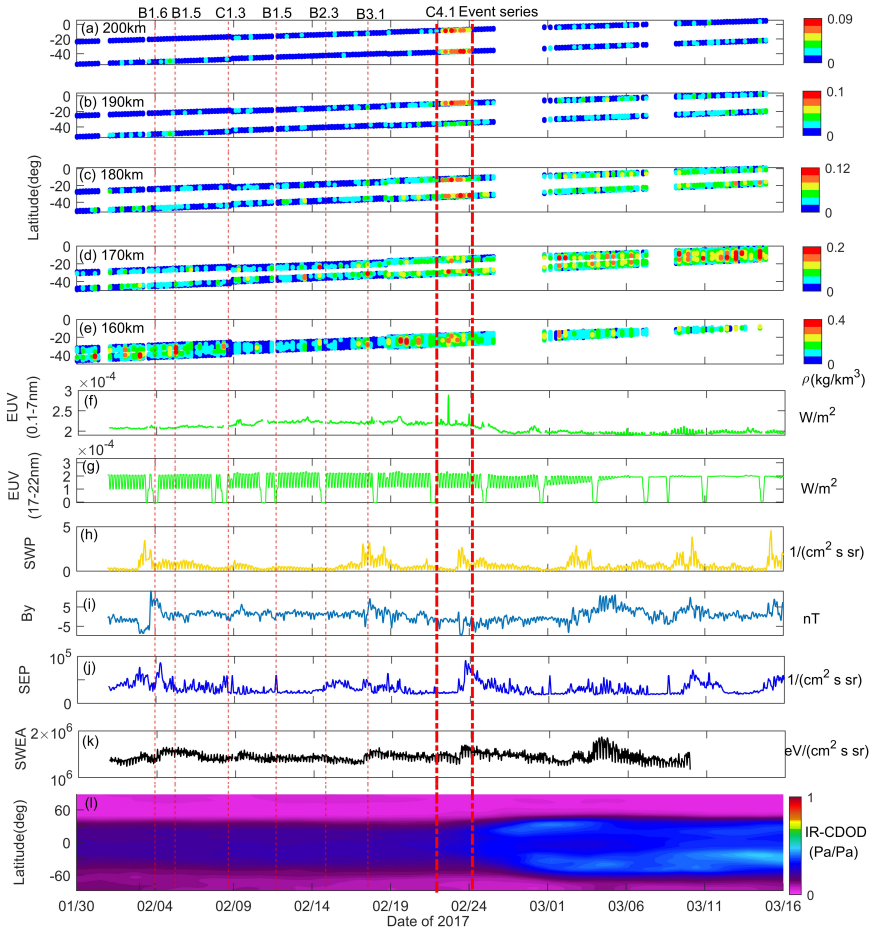

Figure 6. Martian thermospheric density perturbations caused by the solar flares are illustrated during February 2017. The first five panels (a-e): density at 160 to 200 km. (f) EUV (0.1-7 nm) are X-rays from the hot solar flares. (g) EUV (17-22 nm) represents EUV emissions from relatively cooler solar flares. (h) SWP is the Solar Wind Pressure. (i) B_y refers to the magnet intensity in y-axis measured by MAG, in which the high-frequency background perturbations has been filtered out. (j) SEP: Solar Energetic Particles. (k) SWEA: Solar Wind Electron Analyzer. (l) IR-CDOD is used evaluate the surface dust storms. The density is measured during nightside (SZA>90°).

The heating rate caused by the 0.1-7 nm X-rays decreases with the altitude whereas the density increases with the height under HE. The energy is absorbed by the atmospheric volatiles when the EUV (0.1-7 nm) goes through the upper layers. The lower boundary of the heating effects by EUV (0.1-7 nm) enhance-

ment is at about 170 km, where the detected density approximates 0.1-0.2 kg km^{-3} that is at the same magnitude as the background variations.

It should be noticed that the density increases are due to energy transportation from dayside since the density observed inbound/outbound during the event series is in the nightside (100°<SZA<115°, bottom panels of Figure 4). The higher background density after 1st March is due to directional solar heating or strong day night transmission as these measurements are made near the day-night terminator (SZA nearby 90°). Some high-density irregularities after 24th February might be related to surface dust storms as the IR-CDOD becomes larger than before (Figure 6l).

4.3 Density responses to the March 2017 B3.3 Solar Flare

The EUV enhancement in 17-22 nm caused by a newborn solar corona (relatively cooler) and the coupling solar flares are shown in Figure 1. The EUV enhancement begins with the B3.3 solar flare on 22nd March (Table 3), of which the fluxes increase from 2×10^{-4} to 2×10^{-3} W m^{-2} in EUV (17-22 nm) during the events (Figure 7g). Then, the density increases 1 to 3 times when the altitude exceeds 180 km (Figure 7a-7e).

Table 3. The Solar Flare Series during 22nd to 24th March 2017

Flare-Class Stage(UTC)	B1.5 3.20	**B3.3 3.22**	B2.8 3.25	C1.3 3.26	C5.1 3.27
Start	:52	**18:21**	:04	:49	:55
Maximum	:59	**18:58**	:13	--:--	:20
End	:06	**19:15**	:19	:08	:24

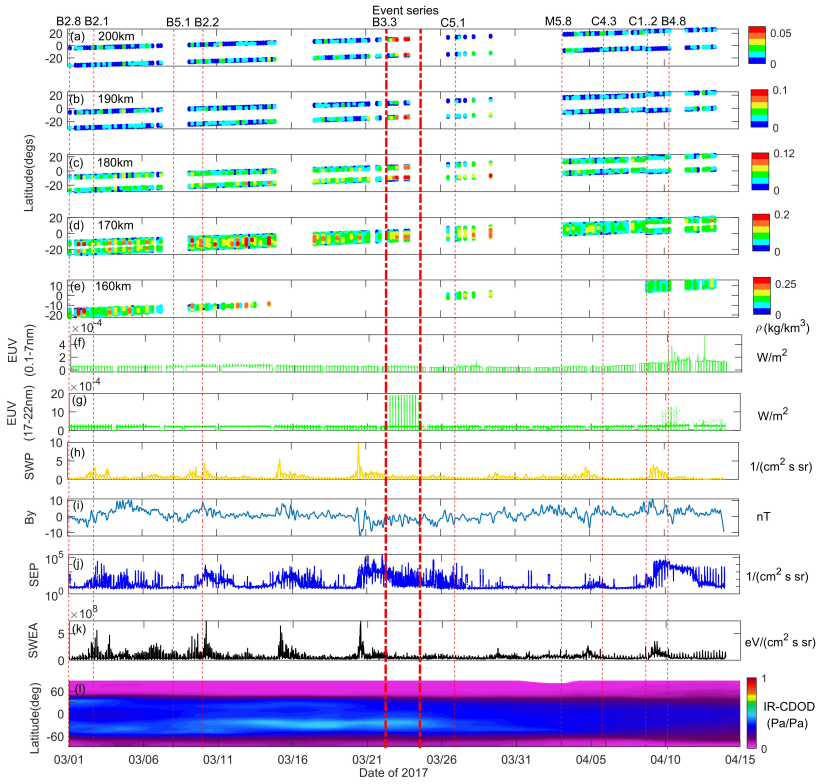

Figure 7. Same as Figure 6 but the solar flares occurred at March 2017 and the density is in dayside (SZA <90°)

The density is heated directly by the 17-22 nm EUV enhancements during the event series. The density derived during this period is in the dayside as shown in Figure 2. Therefore, the background density in Figure 7 is higher than that in Figure 6. It is also shown that the density increases at altitudes lower than 170 km are blanked by the background density distributions. The surface dust storms (Figure 7l) before 27th March could cause higher density irregularities. The magnitude of these irregularities approximates the similar level caused by the EUV (17-22 nm) enhancement. Meanwhile, the moderate EUV enhancement in both two wavelengths on 10th to 14th April B4.8 ~ B1.2 solar flares causes no visible response in Martian thermospheric density, which might be overlapped by the irregularities from the impacts of surface dust storms.

4.4 The effects of the Martian crustal magnetic field

As illustrated in Figure 6, 7 and equation (1), the solar winds and the IMF seem to have no visible effects on shaping the thermal structure of the Martian thermosphere. Only the EUV enhancement coupling with the solar flare

activities could heat the upper atmosphere. However, the plasma-IMF packages from the solar winds and solar flares do affect Mars ionosphere heavily and thus cause heating or cooling of the upper atmospheric ions (Ma et al., 2004, 2014; Lollo et al., 2012; Fallows et al., 2015). Moreover, some latitudinal variations have appeared in Figure 6 and 7, where the density distribution overlaps with the Martian 'butterfly' crustal magnetic field (Figure 3e). What roles do the Martian crustal magnetic field play in shaping the upper thermal structure? In section 4.1 to 4.3, we discuss the ACC data in terms of time-series. It is necessary to consider the same events from the spatial-dependent point of view.

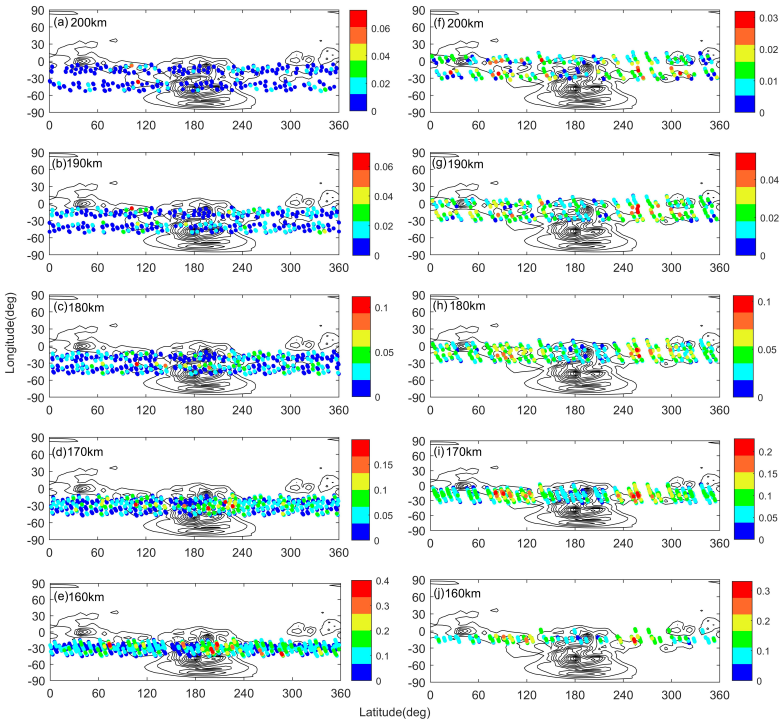

Figure 8. A global spatial distribution map for the ACC background data is shown above. Density during the study events has been removed. (a) to (e): altitudes from 200 to 160 km for the February. (f) to (g): same as (a) to (e) but for March. The colormaps for each figure represent the ACC data-derived density (kg km^{-3}).

The background ACC-derived density and the CMF map are illustrated in Figure 8 during the two events. The background density during the two events overlays with the upper part of the 'butterfly' CMF. For the first event (Figure 8a to 8e), the density is lower in longitude 150°-210°, where the CMF is

strong. The nightside higher irregularities (Figure 8c to 8e) between longitude 180° and 240° are outbound observations (Figure 3e) influenced by the dayside transportation. As shown in the right column of Figure 8 (the March event), the density is lower in the region where the CMF is stronger and vice versa. The CMF has stronger cooling effects on the thermosphere during the day when the sun illuminates the atmosphere.

Figure 9 illustrates the global density distribution during the solar flare events. The density in the left column is measured during the night (SZA ~110°). Therefore, the increased density during the February event series is due to the energy transportation from the dayside heated atmosphere. The density nearby the longitude 180° seems to be lower than elsewhere. Meanwhile, the density in the right column is sampled during the day (SZA<90°), which implies that the density enhancement is mainly due to direct EUV (17-22 nm) heating. The density in the left boundary of the intensive CMF is lower than that in other regions. However, the data available for these two events is limited and more observations are needed to confirm the phenomenon.

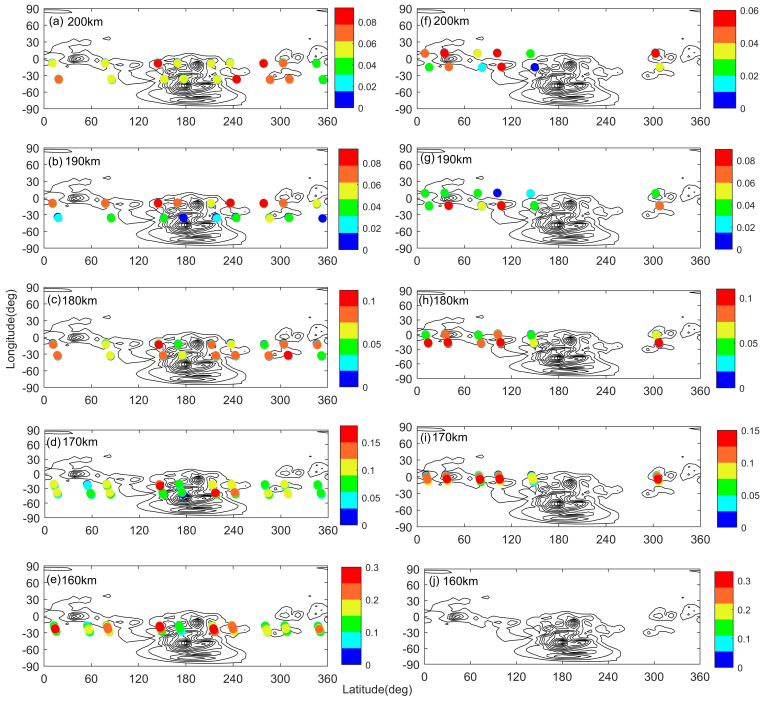

Figure 9. same as Figure 8 but the density is sampled during the studied events

5 Discussions

5.1 The heating of thermosphere density by the solar flares EUV-enhancement

The density increases are due to enhanced EUV fluxes heating accompanied with the solar flares as expected (Elrod et al.,2018; Jain et al., 2018). The February event heats the dayside thermosphere at altitudes more than 170 km with 0.1-7 nm EUV (soft X-rays) fluxes. The density increases 1-3 times more than the background values before the energy is depleted by the increased density at the lower layers. The thermosphere in the nightside nearby the terminator also experiences fast expansion almost synchronously. The observed nightside density increase is due to heating transportation from the dayside, in which the density increases 2-5 times more than the nightside average value (Figure 4 and 6). The average temperature can increase from background 200-300 K to 330-570 K during the event (Figure 10a and 10b). The direct dayside density responses to the solar flares are revealed by the March event (Figure 7). The temperature increases from 200-300 K to 450-600 K (Figure 10c and 10d).

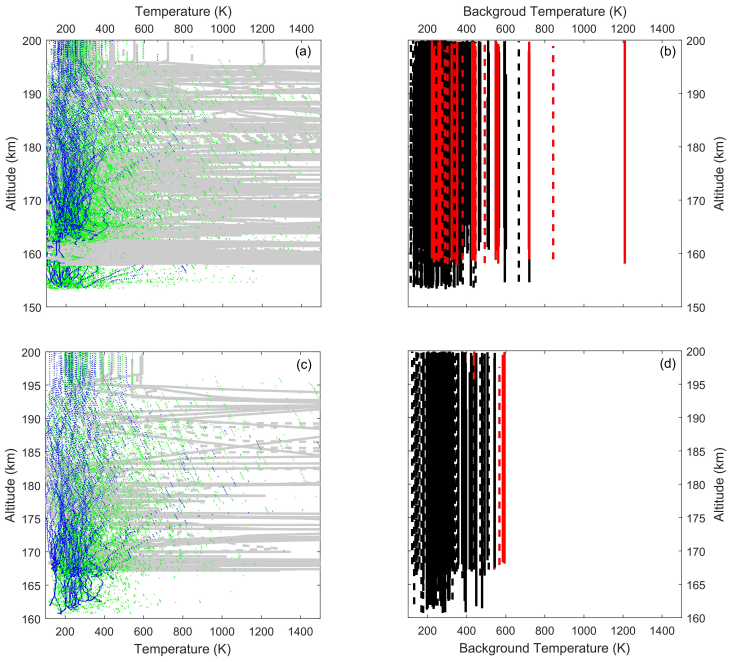

Figure 10. Density-derived temperature is shown above, including (a) temperature profiles and (b) the average values for the February event. Background inbound/outbound values is labeled as green and blue color, respectively. The gray lines (dash/solid for inbound/outbound) are the values during the C4.1

event. The black/red lines refer to the background/heated averaged temperature (Cui et al., 2018; Stone et al., 2018). (c) and (d) for the March event.

The background terms, such as cos (SZA), r^2 and dust storms, not only control the long-term evolution of the thermospheric density, but also have different magnitude contributions to the background variations (Zurek et al., 2017; Liu et al., 2019). The density is sensitive to the projection of the solar fluxes, i.e., the cos (SZA) (Thiemann et al., 2017; Li et al., 2021). The background density experiences an increasing trend due to the decrease of the cos (SZA) during the two events (Figure 4). The dust storms contribute most of the stronger comb-like values between 26^{th} February and 26^{th} March (Figure 6 and 7), which are even higher than the solar flares-induced EUV enhancement impacts at altitudes below 170 km. The influence of r^2 term on the density evolution is slower, and that can be only seen visibly in the time span of at least one Martian Year (Zurek et al., 2017; Liu et al., 2019; Li et al., 2021).

5.2 The role of the Martian CMF

The CMF causes cooling effects on the thermosphere in different degrees as seen in the dayside and nightside (Figure 8). The dayside data distribution represents an obviously lower value near the strong CMF area where the density enhancements are mainly due to direct EUV heating (right column of Figure 8). The nightside data (left column of Figure 8) show a similar phenomenon influenced by the dayside transportation, but there are still high values near strong CMF region (Figure 8c to 8e). These higher irregularities might be corresponded with the day-night transportation.

The reason for the above phenomenon is that strong CMF can shield precipitating fluxes (especially heavy ions) (Hara et al., 2018) where the regional magnetic field formulates more horizontal to the surface (Cui et al., 2018). It potentially enhances the sputtering loss of ambient neutral particles. For the nightside, the CMF might screen the ions' horizontal transport to affect the density distribution indirectly. The dayside CMF has stronger impacts on the density distribution than that during the nightside. It is because that higher EUV fluxes restrain the precipitating fluxes (Martinez et al.,2018).

5.3 The influence on atmospheric escape

The processes caused by the solar flares have been proved to increase the sputtering loss by affecting the ion precipitation (Jakosky et al., 2018). The two moderate events studied in this paper cause unexpected temperature and density fluctuations in the atmosphere (Figure 4, 6, 7 and 10). The heating up of thermospheric density by the solar flare EUV enhancement has important influence on the process of atmospheric escape, especially for Jeans escape (~250 K for H) and hydrodynamic escape (greater than 1000 K for Mars). The atmosphere lifting as a whole powered by EUV heating can lead to hydrodynamic escape of the upper atmosphere (Lammer et al.,2013). The heating process intensifies these two escapes and thus affects thermospheric escape as a factor of long existence.

6 Conclusions

We investigate two moderate (B3.3 and C4.1) solar flares' impacts on the Mars themospheric thermal structure by using MAVEN ACC-derived density/temperature and other sensors' solar-monitoring observations. Both the C4.1 and B3.3 flare couple with EUV enhancement in different wavelength, i.e., EUV (0.1-7 nm, X-rays) and EUV (17-22 nm). The results shows that when the solar activity becomes intense, including the increasing emission of EUV, the high energy particle, energy flow and their magnetic field changes, almost all the density in the detected area experiences an fast and dramatic increase. The increasing of the density is due to the solar EUV heating to the Mars atmosphere. The main conclusions are as follows:

1. The nightside density can be heated up to the same magnitude as dayside does nearly synchronously due to the energy and particles transported from the dayside during the solar flare-induced EUV (0.1-7 nm) enhancement of the February event. Therefore, the averaged nightside background temperature can increase from ~200 to ~350 K, coupling with various scales of density-temperature fluctuation that could be regarded as gravity waves.

2. The direct EUV (17-22 nm) heating during the day of the March event causes density increase for 2-5 times higher than the background values, which is equivalent to a temperature enhancement of 250 K (increases from 250 K to 500 K). The dissipating and braking of gravity waves triggered by the event are the second important heating source, and the temperature can be heated to more than 1000 K.

3. The Mars Crustal Magnetic Field (CMF) can alter the spatial distribution of the background thermal structure, where the region of stronger CMF has a relatively lower density distribution. The closed magnetic lines in the area might could shield the ions to precipitate and screen the ions' horizontal transport.

4. Huge density/temperature fluctuations have been generated during the two events. The increased background temperature can accelerate the Jeans Escape rates of some light species such as atomic Hydrogen (H). The EUV and the coupling gravity wave heating can cause temperature perturbations that could surpass Mars hydrodynamic escape limit (~1000 K).

Data Availability Statement

The MAVEN ACC and EUV datasets used in this paper are available in https://atmos.nmsu.edu/PDS/data/PDS4/MAVEN/acc_bundle/l3/ and https://lasp.colorado.edu/maven/sdc/public/data/sci/euv/l2/. The solar flares recorded by SOHO satellite can be found in https://lasco-www.nrl.navy.mil/daily_mpg/. A quick search for the class of the solar flares can be found at https://www.spaceweatherlive.com/en/archive.html. Other key parameters measured by MAVEN PF and LPW are archived in https://lasp.colorado.edu/maven/sdc/public/pages/plots/kp/kp.html.

The IR-CDOD dataset generated by can be found at http://www-mars.lmd.jussieu.fr/mars/dust_climatology/index.html.

Acknowledgments

The paper is supported by the Scholarship of China Scholarship Council (Grant No: 202008320181), National Natural Science Foundation of China (Grant No:41804151, 42074186), the Startup Foundation for Introducing Talent of NUIST (Grant No: 2019r089) and Key Laboratory of Planetary Sciences Project (Grant No: PSL 1607). This work made use of the High Performance Computing Resource in the Core Facility for Advanced Research Computing at Shanghai Astronomical Observatory.

References

Andersson, L., Ergun, R. E., Delory, G. T., Eriksson, A., Westfall, J., Reed, H., et al. (2015). The Langmuir probe and waves (LPW) instrument for MAVEN. Space Science Reviews, 195(1), 173-198. https://doi.org/10.1007/s11214-015-0194-3Connerney, J. E. P., Espley, J., Lawton, P., Murphy, S., Odom, J., Oliversen, R., & Sheppard, D. (2015). The MAVEN magnetic field investigation. *Space Science Reviews, 195*(1), 257-291. https://doi.org/10.1007/s11214-015-0169-4Cravens, T. E., Rahmati, A., Fox, J. L., Lillis, R., Bougher, S., Luhmann, J., et al. (2017). Hot oxygen escape from Mars: Simple scaling with solar EUV irradiance. *Journal of Geophysical Research: Space Physics, 122*(1), 1102-1116. https://doi.org/10.1002/2016JA023461Cui, J., Yelle, R. V., Zhao, L. L., Stone, S., Jiang, F. Y., Cao, Y. T., et al. (2018). The impact of crustal magnetic fields on the thermal structure of the Martian upper atmosphere. *The Astrophysical Journal Letters, 853*(2), L33. https://doi.org/10.3847/2041-8213/aaa89aCurry, S. M., Luhmann, J. G., Ma, Y. J., Dong, C. F., Brain, D., Leblanc, F., et al. (2015). Response of Mars O+ pickup ions to the 8 March 2015 ICME: Inferences from MAVEN data-based models. *Geophysical Research Letters, 42*(21), 9095-9102. https://doi.org/10.1002/2015GL065304Elrod, M. K., Curry, S. M., Thiemann, E. M. B., & Jain, S. K. (2018). September 2017 solar flare event: Rapid heating of the Martian neutral upper atmosphere from the X-class flare as observed by MAVEN. *Geophysical Research Letters, 45*(17), 8803-8810. https://doi.org/10.1029/2018GL077729Fallows, K., Withers, P., & Gonzalez, G. (2015). Response of the Mars ionosphere to solar flares: Analysis of MGS radio occultation data. *Journal of Geophysical Research: Space Physics, 120*(11), 9805-9825. https://doi.org/10.1002/2015JA021108Fang, X., Ma, Y., Luhmann, J., Dong, Y., Brain, D., Hurley, D., et al. (2018). The morphology of the solar wind magnetic field draping on the dayside of Mars and its variability. *Geophysical Research Letters, 45*(8), 3356-3365. https://doi.org/10.1002/2018GL077230

Fang, X., Pawlowski, D., Ma, Y., Bougher, S., Thiemann, E., Eparvier, F., et al. (2019). Mars upper atmospheric responses to the 10 September 2017 solar flare: A global, time-dependent simulation. *Geophysical Research Letters, 46*(16), 9334-9343. https://doi.org/10.1029/2019GL084515

Forget, F., Montmessin, F., Bertaux, J. L., González-Galindo, F., Lebonnois,

S., Quemerais, E., et al. (2009). Density and temperatures of the upper Martian atmosphere measured by stellar occultations with Mars Express SPICAM. *Journal of Geophysical Research: Planets, 114*(E1), E01004. https://doi.org/10.1029/2008JE003086

Jakosky, B. M., Grebowsky, J. M., Luhmann, J. G., Connerney, J., Eparvier, F., Ergun, R., et al. (2015). MAVEN observations of the response of Mars to an interplanetary coronal mass ejection. *Science, 350*(6261), aad0210. https://doi.org/10.1126/science.aad0210

Jakosky, B. M., Slipski, M., Benna, M., Mahaffy, P., Elrod, M., Yelle, R., et al. (2017). Mars' atmospheric history derived from upper-atmosphere measurements of 38Ar/36Ar. *Science, 355*(6332), 1408-1410. https://doi.org/10.1126/science.aai7721

Jakosky, B. M., Brain, D., Chaffin, M., Curry, S., Deighan, J., Grebowsky, J., et al. (2018). Loss of the Martian atmosphere to space: Present-day loss rates determined from MAVEN observations and integrated loss through time. *Icarus, 315*, 146-157. https://doi.org/10.1016/j.icarus.2018.05.030

Jain, S. K., Deighan, J., Schneider, N. M., Stewart, A. I. F., Evans, J. S., Thiemann, E. M. B., et al. (2018). Martian thermospheric response to an X8. 2 solar flare on 10 September 2017 as seen by MAVEN/IUVS. *Geophysical Research Letters, 45*(15), 7312-7319. https://doi.org/10.1029/2018GL077731

Hara, T., Luhmann, J. G., Leblanc, F., Curry, S. M., Halekas, J. S., Seki, K., et al. (2018). Evidence for crustal magnetic field control of ions precipitating into the upper atmosphere of Mars. *Journal of Geophysical Research: Space Physics*, *123*(10), 8572-8586. https://doi.org/10.1029/2017JA024798

Lammer, H., Chassefière, E., Karatekin, Ö., Morschhauser, A., Niles, P. B., Mousis, O., et al. (2013). Outgassing history and escape of the Martian atmosphere and water inventory. *Space Science Reviews, 174*(1), 113-154. https://doi.org/10.1007/s11214-012-9943-8

Li, Y., Liu, J., & Jin, S. (2021). Horizontal Internal Gravity Waves in the Mars Upper Atmosphere from MAVEN ACC and NGIMS Measurements. *Journal of Geophysical Research: Space Physics, 126*(1), e2020JA028378. https://doi.org/10.1029/2020JA028378

Liu, J., Jin, S., & Li, Y. (2019). Seasonal Variations and Global Wave Distributions in the Mars Thermosphere From MAVEN and Multisatellites Accelerometer-Derived Mass Densities. *Journal of Geophysical Research: Space Physics, 124*(11), 9315-9334. https://doi.org/10.1029/2019JA026720

Lollo, A., Withers, P., Fallows, K., Girazian, Z., Matta, M., & Chamberlin, P. (2012). Numerical simulations of the ionosphere of Mars during a solar flare. *Journal of Geophysical Research: Space Physics, 117*(A5), A05314. https://doi.org/10.1029/2011JA017399

Ma, Y., Nagy, A. F., Sokolov, I. V., & Hansen, K. C. (2004). Three-dimensional, multispecies, high spatial resolution MHD studies of the solar wind interaction with Mars. *Journal of Geophysical Research: Space Physics, 109*(A7), A07211. https://doi.org/10.1029/2003JA010367

Ma, Y., Fang, X., Nagy, A., Russell, C., & Toth, G. (2014). Martian ionospheric responses to dynamic pressure enhancements in the solar wind. *Journal of Geophysical Research: Space Physics, 119*(2), 1272-1286. https://doi.org/10.1002/2013JA019402

Mahajan, K., Lodhi, N. K., & Singh, S. (2009). Ionospheric effects of solar flares at Mars. *Geophysical Research Letters, 36*(15), L15207. https://doi.org/10.1029/2009GL039454

Martinez, A., Leblanc, F., Chaufray, J.-Y., Modolo, R., Witasse, O., Dong, Y., et al. (2019). Influence of extreme ultraviolet irradiance variations on the precipitating ion flux from MAVEN observations. *Geophysical Research Letters, 46*(13), 7761-7768. https://doi.org/10.1029/2019GL083595

Montabone, L., Millour, E., Forget, F., Spiga, A., Kass, D. M., & Kleinbohl, A. (2019). Martian year 34 climatology of the atmospheric column dust optical depth [data set]. *ESPRI/IPSL.* https://doi.org/10.14768/20191217001.1.

Romanelli, N., Modolo, R., Leblanc, F., Chaufray, J. Y., Martinez, A., Ma, Y., et al. (2018). Responses of the Martian magnetosphere to an interplanetary coronal mass ejection: MAVEN observations and LatHyS results. *Geophysical Research Letters, 45*(16), 7891-7900.

https://doi.org/10.1029/2018GL077714Romanelli, N., DiBraccio, G., Modolo, R., Leblanc, F., Espley, J., Gruesbeck, J., et al. (2019). Recovery timescales of the dayside Martian magnetosphere to IMF variability. *Geophysical Research Letters, 46*(20), 10977-10986. https://doi.org/10.1029/2019GL084151Stone, S. W., Yelle, R. V., Benna, M., Elrod, M. K., & Mahaffy, P. R. (2018). Thermal structure of the Martian upper atmosphere from MAVEN NGIMS. Journal of Geophysical Research: Planets, 123(11), 2842-2867. https://doi.org/10.1029/2018JE005559Thiemann, E. M. B., Eparvier, F. G., Andersson, L. A., Fowler, C. M., Peterson, W. K., Mahaffy, P. R., et al. (2015). Neutral density response to solar flares at Mars. *Geophysical Research Letters, 42*(21), 8986-8992. https://doi.org/10.1002/2015GL066334Thiemann, E. M., Chamberlin, P. C., Eparvier, F. G., Templeman, B., Woods, T. N., Bougher, S. W., & Jakosky, B. M. (2017). The MAVEN EUVM model of solar spectral irradiance variability at Mars: Algorithms and results. *Journal of Geophysical Research: Space Physics, 122*(3), 2748-2767. https://doi.org/10.1002/2016JA023512Thiemann, E., Andersson, L., Lillis, R., Withers, P., Xu, S., Elrod, M., et al. (2018). The Mars topside ionosphere response to the X8. 2 solar flare of 10 September 2017. *Geophysical Research Letters, 45*(16), 8005-8013. https://doi.org/10.1029/2018GL077730Withers, & Paul. (2006). Mars Global Surveyor and Mars Odyssey Accelerometer observations of the Martian upper atmosphere during aerobraking. *Geophysical*

Research Letters, 33(2), L02201. https://doi.org/10.1029/2005GL024447Zurek, R., , R. T., Baird, D., , M. Z. J., & Bougher, a. S. W. (2015). Application of MAVEN Accelerometer and Attitude Control Data to Mars Atmospheric Characterization. *Space Science Reviews, 195*(1-4), 303-317. https://doi.org/10.1007/s11214-014-0095-x

Zurek, R., Tolson, R., Bougher, S., Lugo, R., Baird, D., Bell, J., & Jakosky, B. (2017). Mars thermosphere as seen in MAVEN accelerometer data. *Journal of Geophysical Research: Space Physics, 122*(3), 3798-3814. https://doi.org/10.1002/2016JA023641